International Journal of Naval Architecture and Ocean Engineering 10 (2018) 250–258

Contents lists available at ScienceDirect

International Journal of Naval Architecture and Ocean Engineering

journal homepage: http://www.journals.elsevier.com/international-journal-of-naval-architecture-and-ocean-engineering/

Preliminary optimal configuration on free standing hybrid riser

Kyoung-Su Kim [a], Han-Suk Choi [a], Kyung Sung Kim [b, *]

[a] Graduate School of Engineering Mastership, POSTECH, Pohang, South Korea
[b] Department of Naval Architecture and Ocean Engineering, Tongmyong University, Busan, South Korea

ARTICLE INFO

Article history:
Received 10 March 2017
Received in revised form
11 October 2017
Accepted 31 October 2017
Available online 23 February 2018

Keywords:
Free standing hybrid riser
Hybrid riser system
Buoyancy can
Flexible jumper
Deepwater
Multi-body dynamics

ABSTRACT

Free Standing Hybrid Riser (FSHR) is comprised of vertical steel risers and Flexible Jumpers (FJ). They are jointly connected to a submerged Buoyancy Can (BC). There are several factors that have influence on the behavior of FSHR such as the span distance between an offshore platform and a foundation, BC up-lift force, BC submerged location and FJ length.

An optimization method through a parametric study is presented. Firstly, descriptions for the overall arrangement and characteristics of FSHR are introduced. Secondly, a flowchart for optimization of FSHR is suggested. Following that, it is described how to select reasonable ranges for a parametric study and determine each of optimal configuration options. Lastly, numerical analysis based on this procedure is performed through a case study. In conclusion, the relation among those parameters is analyzed and non-dimensional parametric ranges on optimal arrangements are suggested. Additionally, strength analysis is performed with variation in the configuration.

1. Introduction

In recent years, oil & gas field developments have increased in deep water. A hybrid riser is one of the field-proven concept for the deepwater development. This concept consists of Flexible Jumpers (FJ), vertical bundle of rigid riser and sub-surface Buoyancy Can (BC). The BC at the top of the steel riser is located deep enough to avoid critical hydrodynamic loading on the riser.

In addition, with steel riser decoupled from platform motion, the hybrid riser system has benefits in fatigue damage and payloads. However, this concept has limitations in engineering, manufacturing cost for complex components and bottom assembly connection on the seabed.

Several pieces of research into on its configuration have been performed. Dingwall (1997) observed that the FPU should be kept certain distance away from a riser base due to interference issues. Dingwall (1997) also explained the main factors for the BC's location, such as wave induced motions as well as interference between the BC and any of mooring lines. Fernandes et al. (1999) suggested a method to calculate the critical flexible jumper length using the consistent catenary concept, which has minimum tension at the end of the FJ. This length led to an economical approach in flexible jumper design. McGrail and Lim (2004) discussed several factors for global arrangements. In addition, structural characteristics on FSHR were analyzed with strength and fatigue analysis. Song et al. (2010) suggested the design flowchart for FSHR considering the complexity of the system and interface with manufacture and installation. Qin et al. (2011) suggested an optimum configuration design of the FSHR through parametric sensitivity analysis with single-variable control. Kang et al. (2012) suggested the method to determine the size of the BC considering key elements: the ratio of the length to the outer diameter of BC (L/D of BC), Top Tension Factor (TTF), the number of compartments, inner stem pipe and BC strength.

The main objectives of this paper are to propose the procedure for optimal configuration of FSHR and select optimal FSHR models through a case study. Then, useful non-dimensional parameters, which are span distance, submerged buoyancy can water depth and size, for preliminary design are suggested to provide guidance on the structural analysis of steel riser including optimization. Also, structural effects on the steel riser are investigated with variations of global arrangements (see Fig. 1).

2. Methodology

2.1. Flow chart with global arrangement of FSHR

There are a few key parameters which influence the global

* Corresponding author.
E-mail address: keiuskim@tu.ac.kr (K.S. Kim).
Peer review under responsibility of Society of Naval Architects of Korea.

https://doi.org/10.1016/j.ijnaoe.2017.10.012

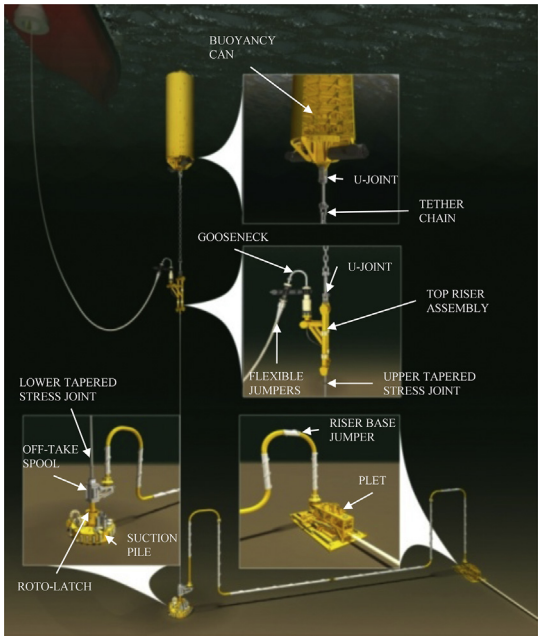

Fig. 1. Main components for FSHR concept (Song and Streit, 2011).

FSHR's arrangement, as can be seen below as Fig. 2.

- Submerged buoyancy can water depth
- Buoyancy can size
- Span distance
- Flexible jumper length (L_{FJ})
- Field interference

With these parameters, an overall flowchart for the design procedure on the optimal configuration is introduced as shown in Fig. 3. According to Fig. 3, the flow chart, it is seen that the depth of buoyancy can be determined by initial value, and then the span size and length and diameter of buoyancy can estimated by Metocean data and buoyancy can data. In the first criterion of them, convergence test would be run until all parameter met the criteria. And it proceed to second stage which is fatigue analysis. If it is failed to satisfy the fatigue criterion, whole procedure start over. The final stage on this procedure is cost estimation.

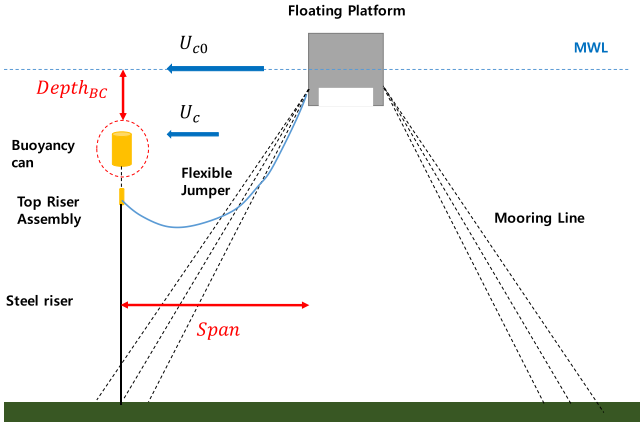

Fig. 2. Global arrangement of FSHR components.

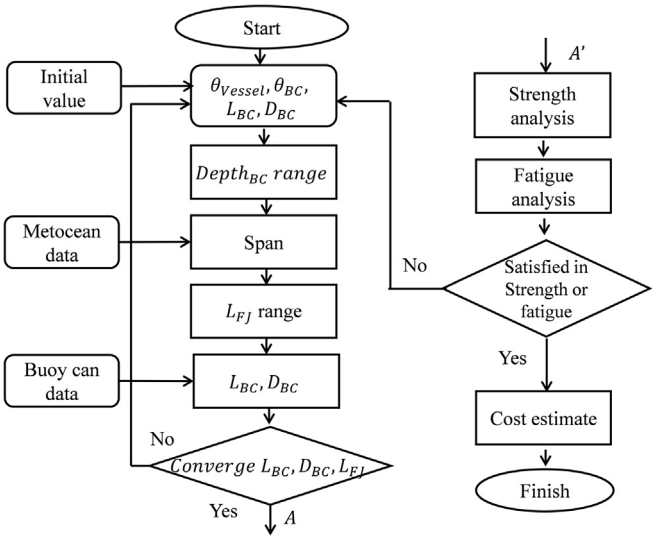

Fig. 3. Overall flowchart for optimal configuration.

2.2. Buoyancy can depth

First of all, basic design data such as the hang-off angle of the flexible jumper and the buoyancy design data are assumed to be reasonable value or brought from previous engineering experience. A BC is normally located deep enough to avoid critical wave and current loading. In a view of engineering experience, it is normally located between 50 and 150 m below free surface. In detail, it depends on wave and current loading in the environmental conditions for the certain field (Kang et al., 2012; Roveri et al., 2008).

According to Dingwall (1997), the BC should be located at which there is 5% wave energy relative to that on the free surface for fatigue issue. Thus, BC water depth where it has 5% of the acceleration of wave particle compared to that on the free surface is considered standard water depth (100%) as in Eq. (1) using deep water approximation, and then ranges of the BC water depth are divided into 100–250% at an interval of 5%.

$$a_x = kgA \times e^{ky} \times \sin(kx - \omega t)$$

$$\omega = \frac{2\pi}{T_p}(\text{wave angular frequency})$$

$$k = \frac{2\pi}{\lambda}(\text{wave number}) \tag{1}$$

where A and y are wave amplitude and water depth. T_p is wave period and λ is wavelength. g is a gravitational acceleration. x is x -coordinate of a wave particle.

2.3. Span distance

Span is the distance measured from the riser base on the seabed to a fairlead of FPU. For the interference aspect, the BC should not come into contact with other structures such as FPU and mooring lines. Thus, span distance can be expressed as Eq. (2) and Fig. 4.

$$\text{Span} = WC_{FPU} + WC_{BC} + Margin \tag{2}$$

where WC_{FPU} and WC_{BC} mean the watch circle (maximum lateral offset) of the FPU and the BC, respectively. The margin is an additional offset distance for the purpose of marginal safety factor for

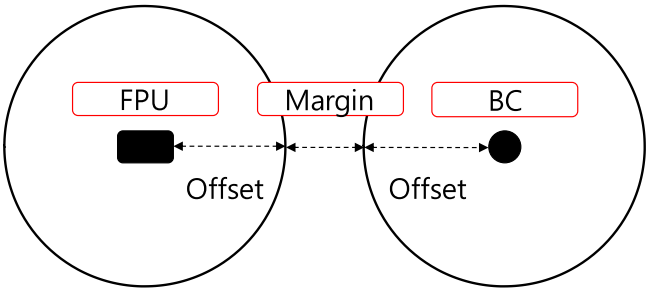

Fig. 4. Brief description for span distance.

interference and structural issues.

2.4. Flexible jumper length

For decoupling effect from vessel motions, the FJ should be long enough so that minimum tension is applied at the ends of the jumper.

Fernandes et al. (1999) introduced the critical jumper length equation for having the minimum tension in the same height at the ends as presented in Eq. (3).

$$L_{crit} \cong 1.2577s \tag{3}$$

where L_{crit} is critical FJ length and s is span distance.

The critical flexible jumper length of FSHR should be determined with span distance under the north direction of the environmental condition in Fig. 6, because L_{crit} from span for north condition is long enough to prevent rapidly increasing tension as shown in Fig. 5. The floater has 4 fairlead points and each point has 3 mooring lines to avoid drifting away.

With this critical jumper length as a standard length, a minimum FJ length with the minimum tension can be determined in different BC water depth through the sensitivity study.

2.5. Buoyancy can size

The BC is designed to be pressure-balanced where the internal pressure is slightly higher than the external hydrostatic pressure. In addition, divided compartments prevent fatal buoyancy loss all at once.

According to Kang et al. (2012), the preliminary design flow for

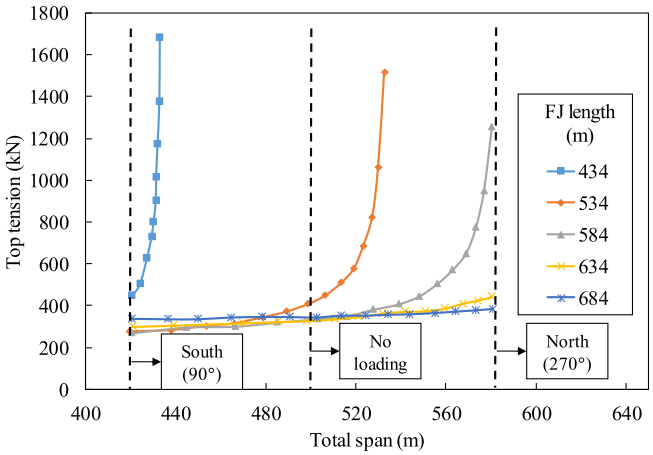

Fig. 5. Critical length applied to several conditions (Fernandes et al., 1999).

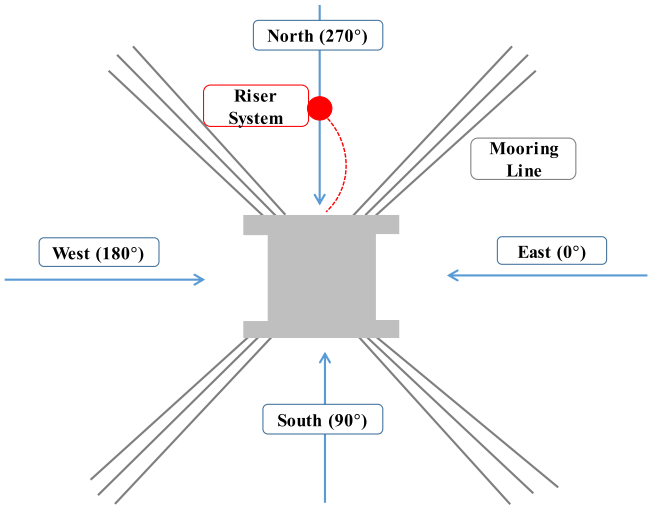

Fig. 6. Wave & current direction.

the BC is below:

Step 1) Generate all data related to the BC design. In the beginning, reasonable assumptions for design parameters are made based on previous project experience.
Step 2) Implement a sensitivity study for the effect of L/D of the BC to the drag force and the weight. Ranges of L/D can be found out by analyzing trends on both drag force and weight corresponding to L/D. In this paper, L/D ratio from a previous project is used.
Step 3) Collect the components weight information based on the design basis such as the weight of the steel riser, the FJ, tether chains, and the TRA. Calculate the required net up-lift force, W_{BC} through Eq. (4). Then, the length of L and D can be obtained from the ratio of the BC weight to the displaced water weight from engineering experience in Eq. (5) and L/D of the BC from step 2. The Typical Top Tension Factor (TTF) in Eq. (4) is 1.5 or more in case of no contingency compartments inside BC. So, in this paper, ranges of TTF for a sensitivity study are from 1.125 to 2.25 at an interval of 0.125.

$$TTF = \frac{W_{BC} - W_{Tether} - W_{TRA} - W_{Jumper}/3}{W_{Rigid\ \ pipe} + W_{RR\ \ Coating} + W_{RR\ \ Fluid} - W_{RR\ \ Displacement}} \tag{4}$$

$$\frac{W_{BC\ \ in\ \ air}}{W_{Displaced\ \ water}} = \frac{W_{BC\ \ in\ \ air}}{\rho_w \frac{\pi}{4} D^2 L} = 0.3 \tag{5}$$

where ρ_w is seawater density. W_{BC}, W_{Tether}, W_{TRA}, W_{Jumper} mean the weight of submerged BC, submerged tether chain and submerged top riser assembly, respectively. $W_{Rigid\ \ pipe}$, $W_{RR\ \ Coating}$, $W_{RR\ \ Fluid}$ and $W_{RR\ \ Displacement}$ represent the dry weight of steel riser, riser coating and fluid inside riser and displaced water weight by riser. The value of Eq. (5) is set to 0.3 and it was determined by referring corresponding experiment conducted by Kang et al. (2012).

Briefly, BC length and diameter can be determined from L/D ratio, BC weight ratio and weight of components from Section 3.2.

3. Application to the case study

3.1. Software for the case study

In this paper, OrcaFlex was used to implement non-linear multi-

body simulation. OrcaFlex is specialized in time domain analysis for the offshore structures, e.g. platform, pipelines, buoys, winches, etc.

3.2. Design of basis

This procedure was applied into the case study based on the Rocandor P-52 FSHR. There are main components particulars such as steel riser, BC, FJ listed in Tables 1–3 (Roveri et al., 2008). Semi-submergible was selected as FPU.

Specifically, when it comes to the design of FJ, it consists of multiple layers having different properties in Fig. 8. It leads to its unique bending behavior called hysteresis bending stiffness curve can be obtained by referring Kebadze (2000) as described in Fig. 7. This non-linear bending response was used in order to avoid an overestimate in response (Tan et al., 2009).

Also, Tapered Stress Joints (TSJ) and flex-joints were typically used at both ends of the riser to restrain the excessive bending stress since the connection part of steel riser are typically vulnerable to structural stress. In the similar way, bend stiffeners were attached to restrict the excessive bend radius of the jumper at the vessel and gooseneck termination.

3.3. Environmental conditions

Gulf of Mexico (GOM) field data and 1800m water depth were considered in the case study as presented in Table 4.

In the GOM, a loop current affects across the entire water depth, which is the main cause for fatigue damage on the steel riser with VIV effect. Fig. 9 presents the loop current profile in the GOM.

3.4. Optimal configuration selection

As a first step, it was assumed that the hang-off angles were 10° and 35° at the FPU and gooseneck respectively, quoted from the P-52 FSHR. BC length and diameter were 34.2 m and 5.45 m respectively as initial values.

Table 1
Steel riser properties.

Parameter	Value
Outside diameter (mm)	457.2
Wall thickness (mm)	15.8
Material standard based on API Spec 5L	X-65
Thermal insulation thickness (solid PP) (mm)	50
Design pressure (MPa)	10.98

Table 2
Buoyancy can properties.

Parameter	Value
Nominal length (m)	34.2
Nominal outside diameter (m)	5.45
Nominal net uplift (operation) (tonne)	536
No. compartments water filled	2
Central stem OD (m)	1.42

Table 3
Flexible jumper properties.

Parameter	Value
Outside diameter (mm)	541.0
Inside diameter (mm)	381
Axial stiffness (kN/m)	1365000
Bending stiffness (kNm^2)	Ref. to M-C curve

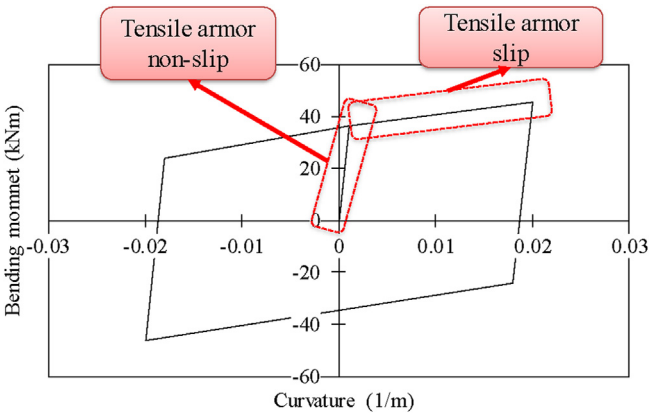

Fig. 7. Theoretical bending moment–curvature curve of 15″ pipe (100 bar inner pressure) (Kebadze, 2000).

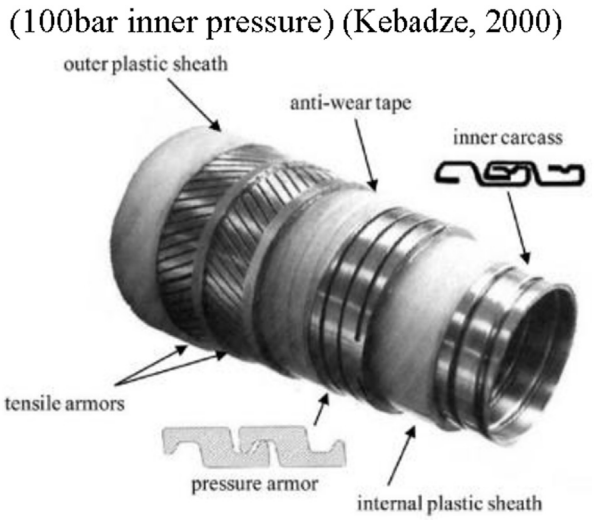

Fig. 8. Typical flexible pipe (Sousa et al., 2012).

Table 4
Metocean data for waves, currents and winds.

Parameter	Winter storm	Wave dominant hurricane	Wind dominant hurricane
Return period [yr.]	10	100	100
Wave			
Significant wave height [m]	6.1	14.1	13.3
Peak spectral period [sec]	11.3 ~ 11.8	14.5 ~ 15.8	14.1 ~ 15.4
Peak enhancement factor [γ]	2.0	2.4	2.4
Wind (1hr, @ 10 m)			
Wind speed [m/s]	16	40	44
Current			
Surface speed [m/s]	0.41	1.86	1.94
Speed at 2nd profile [m/s]	0.39	1.39	1.42
2^{nd}-profile depth [m]	34	39	39
Speed at 3rd profile [m/s]	0.21	0	0
3^{rd}-profile depth [m]	62	74	74
Speed at 4th profile [m/s]	0	N/A	N/A
4^{th} profile depth [m]	95	N/A	N/A

Based on section 2, the values for BC water depth, span and FJ length were obtained with the initial BC size. The standard BC water depth and the corresponding span distance were analyzed

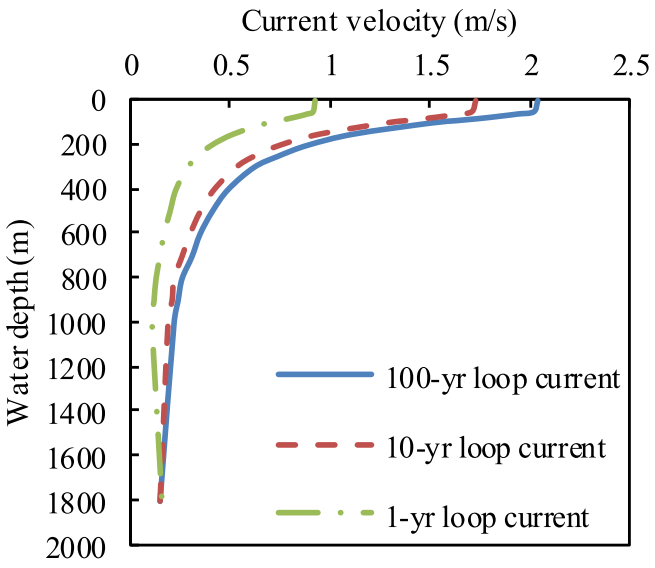

Fig. 9. Loop current profile in the GOM.

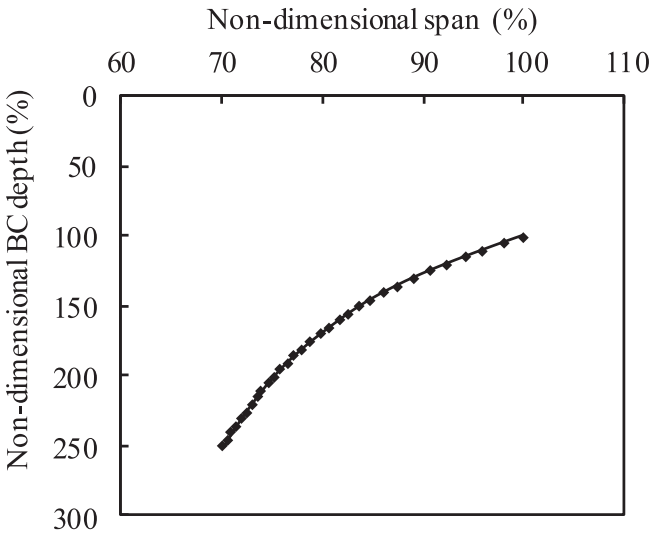

Fig. 10. Tendency between span and **BC water depth**.

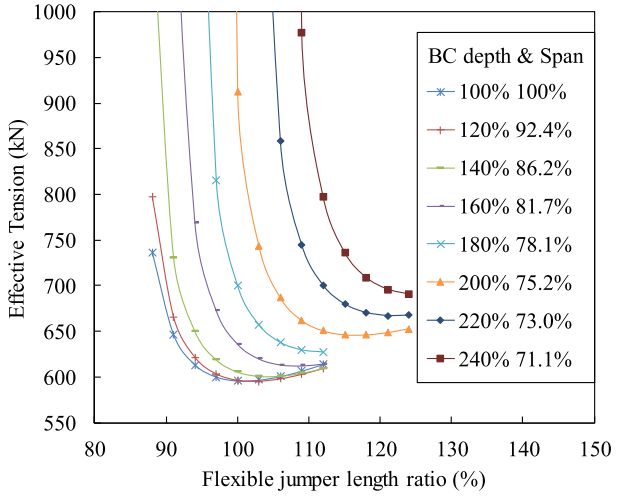

Fig. 11. Effective tension (at FPU) along with non-dimensional FJ ratio.

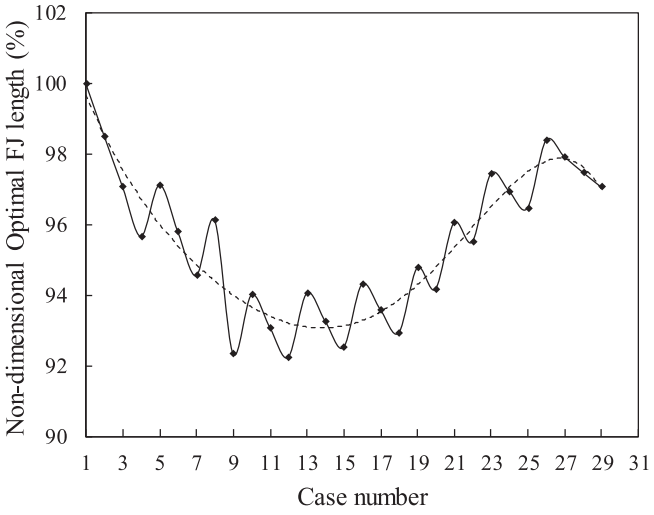

Fig. 12. Non-dimensional optimal flexible jumper length along with non-dimensional **BC water depth**.

under the extreme weather conditions. The offset in 100yr-loop-current caused the longest span distance, because this current could apply significantly the loading up to the BC located in the deep water.

Based on the above results, the BC water depth and span distance are normalized by the standard BC water depth and corresponding span distance from Eqs. (1) and (2) and the relationship was derived. When the BC water depth went deeper, the span distance became shorter due to less current loading. Fig. 10 represents this trend well.

The critical length (L_{crit}) was considered 100% length in the

Table 5
Configuration array with initial values.

Case no.	BC water depth (m)	Span distance (m)	FJ length (m)
1	96.71 (100%)	293.26 (100%)	491.02
2	101.55 (105%)	287.44 (98.0%)	483.70
3	106.38 (110%)	281.80 (96.1%)	476.60
4	111.22 (115%)	276.31 (94.2%)	469.70
5	116.05 (120%)	270.98 (92.4%)	476.88
6	120.89 (125%)	265.95 (90.7%)	470.37
7	125.72 (130%)	261.21 (89.1%)	464.23
8	130.56 (135%)	256.87 (87.6%)	471.96
9	135.39 (140%)	252.84 (86.2%)	453.38
10	140.23 (145%)	249.06 (84.9%)	461.56
11	145.07 (150%)	245.68 (83.8%)	457.04
12	149.90 (155%)	242.57 (82.7%)	452.89
13	154.74 (160%)	239.69 (81.7%)	461.77
14	159.57 (165%)	236.91 (80.8%)	457.95
15	164.41 (170%)	234.20 (79.9%)	454.24
16	169.24 (175%)	231.56 (79.0%)	463.03
17	174.08 (180%)	229.10 (78.1%)	459.56
18	178.91 (185%)	226.77 (77.3%)	456.27
19	183.75 (190%)	224.57 (76.6%)	465.31
20	188.59 (195%)	222.54 (75.9%)	462.39
21	193.42 (200%)	220.64 (75.2%)	471.62
22	198.26 (205%)	218.85 (74.6%)	468.97
23	203.09 (210%)	217.22 (74.1%)	478.41
24	207.93 (215%)	215.64 (73.5%)	476.01
25	212.76 (220%)	214.10 (73.0%)	473.67
26	217.60 (225%)	212.61 (72.5%)	483.08
27	222.43 (230%)	211.16 (72.0%)	480.81
28	227.27 (235%)	209.77 (71.5%)	478.65
29	232.11 (240%)	208.45 (71.1%)	476.59
30	236.94 (245%)	207.19 (70.6%)	474.62
31	241.78 (250%)	205.97 (70.2%)	472.73

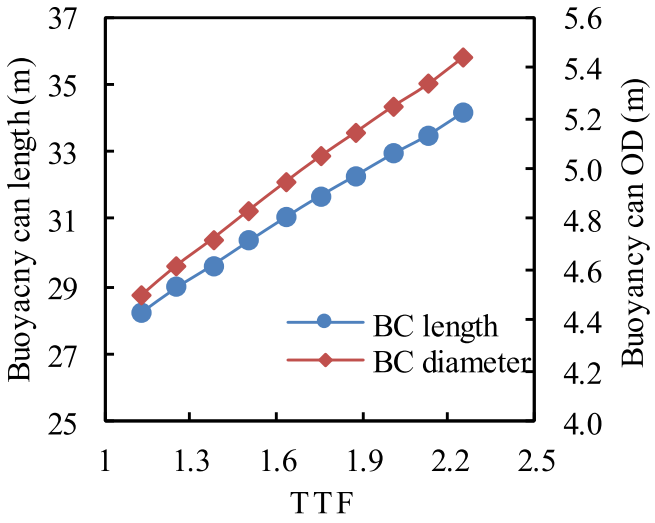

Fig. 13. BC length and diameter corresponding to TTF.

sensitivity study as in section 2.4. However, FJ length should be longer than L_{crit} in order to get the minimum tension at the end of FJ as BC water depth gets deeper. Thus, the FJ length ratio ranged from 88 to 124% at an interval of 3% at each pair of BC water depth and the corresponding span distance case. The range of FJ length was determined by taking minimum values of effective tension in each case through numerical test such like trial and error method. Fig. 11 shows that FJ length ratio has to increase to have minimum effective tension in each case.

$$\text{FJ length raito}(\%) = \frac{FJ\ length}{L_{crit}(span)} \times 100 \tag{6}$$

Fig. 12 shows the flexible jumper length satisfied with the minimum effective tension at each pairs of BC water depth and FJ length. The results are summarized in Table 5.

As a result absolute FJ length decreased as L_{crit} got shorter with shorter span distance up to case 12 in Fig. 12. However, beyond this point, the FJ length increases to satisfy the minimum tension as BC gets deeper. Based on these outcomes, the minimum optimal FJ length in that case of 155% of the BC water depth, which means that 155% of the standard BC water depth, and 82.7% of span distance was selected for economic reasons.

For sizing BC, the ratio of L and D of the BC was assumed to be 6.27 from the P-52 FSHR project. In addition, it was also quoted that there were 16 compartments with 56 in. OD central stem and 0.5 in. wall thickness. There were two water-filled compartments in case of an accident.

Ranges of TTF for the sensitivity study were from 1.125 to 2.25 at an interval of 0.125. The procedure above was iterated until the BC size converged. As a result, the L and D of the BC were proportional to TTF, since an increment of TTF affected the buoyancy force directly. Fig. 13 shows the results for the BC size with a variation of TTF.

This whole procedure is described briefly in Fig. 14, and the results at each TTF are summarized with ten optimal configuration options represented by TTF values in Table 6.

4. Results and discussions

4.1. Tendency for optimal configuration options

Based on the optimal configuration options in section 3, trends can be clearly shown with TTF representing options as described in Fig. 15. Fig. 16 shows the trend of individual parameters. As TTF, i.e., net lift force increased, the BC tended to be located closer to the free surface. When it came to BC water depth, it had stagnant points at

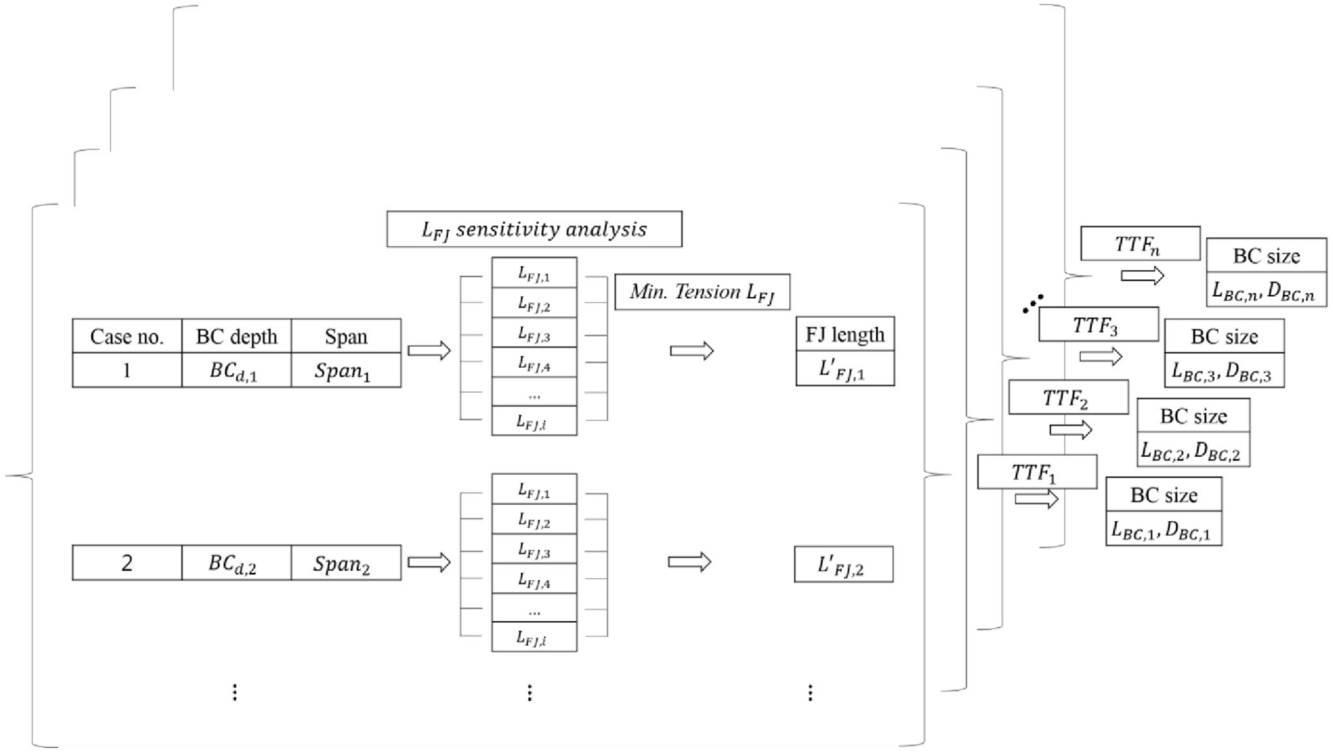

Fig. 14. Overall procedure for determination of optimal configuration.

Table 6
Results for optimal configuration models.

Model no.	TTF	BC water depth (m)	Span (m)	L_{FJ} (m)	L_{BC} (m)	D_{BC} (m)	Net up-lift (te)	Ballast water (te)
1	1.125	193.4	296.8	531.0	28.1	4.4	266.2	53.7
2	1.250	193.4	280.3	514.0	28.9	4.6	288.0	58.6
3	1.375	193.4	269.4	502.4	29.6	4.7	308.1	63.0
4	1.500	188.6	263.2	493.9	30.3	4.8	330.5	68.0
5	1.625	183.7	258.6	487.7	31.0	4.9	353.2	73.1
6	1.750	178.9	255.4	483.2	31.6	5.0	375.9	78.3
7	1.875	178.9	249.7	475.5	32.2	5.1	397.9	83.2
8	2.000	174.1	248.3	473.5	32.9	5.2	421.1	88.4
9	2.125	174.1	244.0	467.7	33.4	5.3	443.1	93.3
10	2.250	169.2	242.9	466.1	34.1	5.4	470.3	99.5

early TTF values due to too low BC up-lift force. In terms of span distance, it got shorter due to reduction of BC offset. This made the FJ length getting shorter.

4.2. Non-dimensional parameter for preliminary design

Non-dimensional parameters were suggested for a preliminary configuration of FSHR.

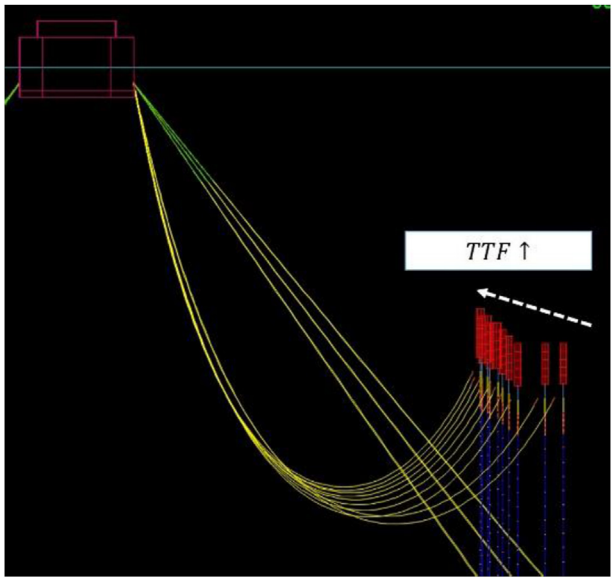

Fig. 15. Global arrangement varying in options.

The first parameter was the ratio of FJ length and span distance which ranged from 1.87 to 1.93.

The second parameter was the ratio of span distance and BC water depth which ranged from 1.43 to 1.53. Except for the ratio in the early TTF having stagnant BC water depth, it was nearly a constant value of 1.42.

Lastly, there was a non-dimensional parameter which represented the ratio of the drag force to the BC from the current and BC buoyancy force as presented in Eq. (7). This ratio was around 0.13 and implied the relation between loop-current speed at certain BC water depth and BC size. These are presented in Fig. 17.

$$\frac{Drag\ \ force}{Buoyancy} = \frac{\frac{1}{2}\rho_w C_d U_c^2 DL}{\frac{\pi}{4}\rho_w g D^2 L} = \frac{2C_d U_c^2}{\pi g D} = C_0 \frac{U_c^2}{gD} \tag{7}$$

where C_d and C_0 are drag coefficient and $2C_d/\pi$. U_c is current speed. g is gravitational acceleration.

4.3. Structural analysis

In the case study, operating (OP) and extreme (EX) load cases in Table 7 were considered for strength analysis. To consider the motion of semi-submergible, its Response Amplitude Operator (RAO) and Quadratic Transfer Function (QTF) were used from WAMIT software. The offset of FPU was mainly more affected by wave 2nd order than wave 1st order. For simplification, strength analysis was implemented under 4 environmental loading direction, i.e., North, east, west and south directions as shown in Fig. 6.

In this section, steel riser was focused in the aspect of structural integrity. However, strength analysis on the FJ and fatigue analysis were not included in this paper. These are typically not a considerable issue because of the flexibility of the jumper and the decoupling effect.

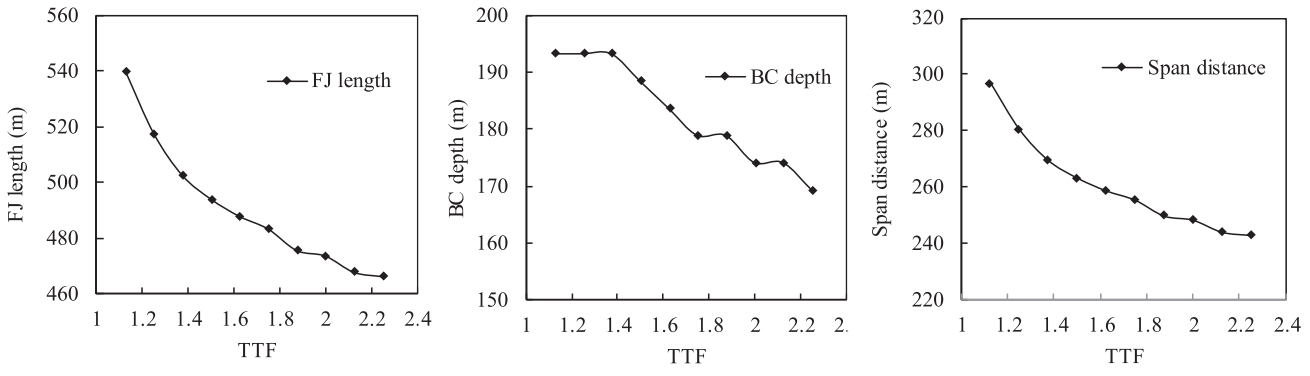

Fig. 16. Variation of main parameters to each TTF values.

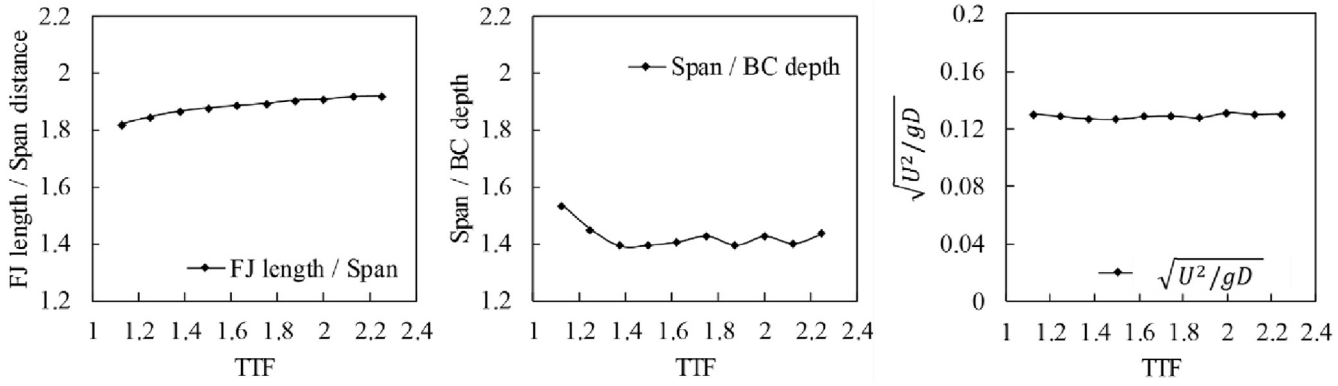

Fig. 17. Non-dimensional parameter to TTF values.

Table 7
Load case matrix for strength and fatigue analysis.

Load Case		Environmental loading	Pressure	Mooring Line Condition	BC condition (flooded compart.)
Strength- Operating	Op1	10-yr Winter Storm	Design	Intact	2
	Op2	10-yr Loop Current			
Strength-Extreme	Ex1	10-yr Winter storm	Design	Damaged	2
	Ex2	100-yr Loop Current		Intact	2
	Ex3	100-yr Hur-Wind Dominant			
	Ex4	100-yr Hur-Wind Dominant			

The results on the maximum Von-Mises stress and load cases are summarized in Fig. 18. Except for Op1 and Ex1 load cases, the highest Von-Mises stress would occur at the bottom due to high bending stress at the lowest TTF, which meant that with the low up-lift force, bending stress at the bottom of the riser was the governing stress across the steel riser. As we can see, Op2 and Ex2, i.e., respectively, 10-yr loop current and 100-yr loop current could cause maximum Von-Mises stress at the bottom of the steel riser up to the 1.375 in TTF, due to the lack of BC's restoring force. Thus, the TTF needed to increase more, especially under the loop-current load case to prevent high bending stress.

In the other words, after TTF, i.e., up-lift force of BC went over 1.375, maximum Von-Mises stress slowly and linearly increased at the top, which means axial stress was the governing stress on the steel riser.

According to the API RP 2RD criteria, it requires following:

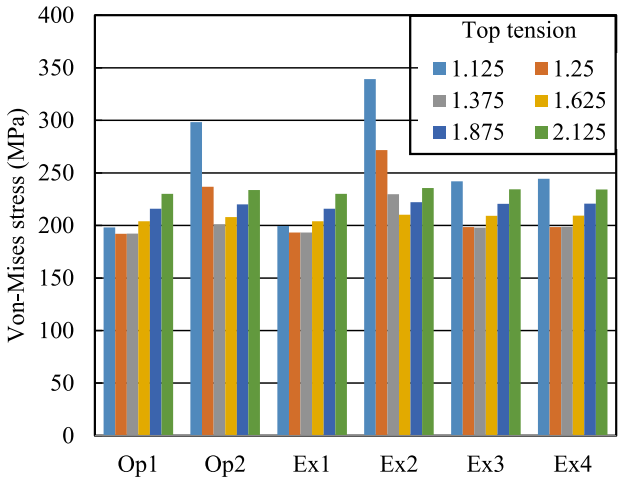

Fig. 18. Maximum Von-Mises stress trends with increases of TTF.

$$\sigma_{API} \leq C_f \sigma_a = C_f C_a \sigma_Y \tag{8}$$

where, σ_{API} and σ_Y mean Von-Mises stress and minimum yield stress. C_f and C_a are design case factor and allowable stress factor listed in Table 8.

According to API (1998), API utilization which is the ratio of σ_{API} and $C_f C_a$ as presented in Eq. (8) should be higher than 1.

The results on API utilization are presented in Fig. 19. According to this graph, there were two critical load cases for Von-Mises stress.

As a result, TTF should be typically greater than 1.375 in the case of two ballast compartments in order to avoid a critical bending stress zone as a governing stress in the preliminary design phase.

4.4. Cost estimate for FSHR

FSHR has a high capital cost (CAPEX) compared to other riser types, e.g., SCR and LWSR, because the FSHR concept requires mechanical complexity in the design and procurement stage. It also has installation difficulties in treating large components and lifting tasks.

The factors influencing the cost estimate are related to the following aspects: materials, fabrication, installation complexity/time and vessel requirements.

As a result, selected global arrangements among optimal configuration options should be satisfied with structural integrity, and then final configuration model can be selected through cost

Table 8
API RP 2RD strength design criteria (API, 1998).

Load case	Design case factor (C_f)	Allowable stress ratio ($C_f C_a$)
Operating	1.00	67%
Extreme	1.20	80%
Survival	1.50	100%
Test	1.35	90%

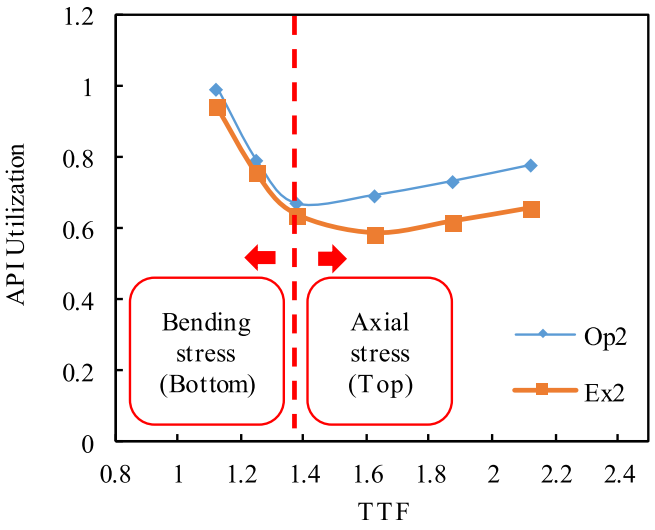

Fig. 19. API utilization trend.

estimate.

5. Conclusions

Through the proposed method for the optimal configuration, how individual parameters could be determined and how they influence each other was shown.

Through the case study, it was figured out that span distance and FJ length tended to exponentially decay as TTF increased. BC water depth also tended to decay overall along with the increases in TTF.

Using these relationships, three non-dimensional parameters could be calculated under GOM field characteristics. Firstly, the ratio of FJ length and span distance ranged from 1.87 to 1.93. Secondly, the ratio of span distance and BC water depth ranged from 1.43 to 1.53. Thirdly, the ratio of the drag force to the BC from the current and BC buoyancy force was around 0.13, and it represented the relationship between the loop-current speed at a certain BC water depth and BC size. They could be useful standards for FSHR in a preliminary design phase.

Structural response on the steel riser was affected by BC size. Bending stress at the riser-base was the most critical and quickly varying at early TTF cases due to the lack of its restoring force. With a large enough up-lift force over a certain TTF value, the axial stress became governing and slowly varying. In conclusion, the buoyancy force of the BC should be large enough for structural integrity.

Acknowledgements

This research was supported by the Technology Innovation Program (10051279, FEED Package of Underwater Pipeline for Oil Production and Transportation, and 10053121, Development of Technology for Decommission and Demolition of 100 m Water Depth Fixed Offshore Plant) funded by the Ministry of Trade, industry & Energy (MI, Korea).

References

API, 1998. Design of Risers for Floating Production Systems (FPSs) and Tension-leg Platforms (TLPs) (API Recommended Practice 2RD). American Petroleum Institute, Washington, USA.

Dingwall, J.R., 1997. The Design of a Deep Water Catenary Riser. Thesis of the degree of doctor philosophy in University of Glasgow.

Fernandes, A.C., Jacob, B.P., Silva, R.M., Carvalho, R.A., Lemos, C.A., 1999. Design of flexible jumpers for deepwater hybrid riser configurations. In: Proceedings of OMAE99, 18th International Conference on Offshore Mechanics and Arctic Enginezzering. St. Johns, Newfoundland, Canada.

Kang, Z., Jia, L., Sun, L., Liang, W., 2012. Design and analysis of typical buoyancy tank riser tensioner systems. J. Mar. Sci. Appl. 11 (No. 3), 351–360.

Kebadze, E., 2000. Theoretical Modelling of Unbonded Flexible Pipe Cross-sections. Doctoral dissertation. South Bank University.

McGrail, J., Lim, F., 2004. SLOR vs. SCR for deepwater applications technical appraisal. In: The Fourteenth International Offshore and Polar Engineering Conference. International Society of Offshore and Polar Engineers.

Qin, W., Kang, Z., Kang, Y., 2011. Free standing hybrid riser global parametric sensitivity analysis and optimum design. In: ASME 2011 30th International Conference on Ocean, Offshore and Arctic Engineering, pp. 569–575.

Roveri, F.E., Velten Filho, A.G., Mello, V.C., Marques, L.F., 2008. The Roncador P52 oil export system-hybrid riser at a 1800m water depth. In: Offshore Technology Conference. Offshore Technology Conference.

Song, R., Stanton, P., Zhou, X., 2010. Engineering design of deepwater free standing hybrid riser. In: ASME 2010 29th International Conference on Ocean, Offshore and Arctic Engineering, pp. 637–649.

Song, R., Streit, P., 2011. Design of the World's deepest hybrid riser system for the cascade & chinook development. In: Offshore Technology Conference. Offshore Technology Conference.

Sousa, J.R.M., Viero, P.F., Magluta, C., Roitman, N., 2012. An experimental and numerical study on the axial compression response of flexible pipes. J. Offshore Mech. Artic Eng. 134 (No. 031703).

Tan, Z., Quiggin, P., Sheldrake, T., 2009. Time domain simulation of the 3D bending hysteresis behavior of an unbonded flexible riser. J. Offshore Mech. Arct. Eng. 131 (No. 031301).